Check for updates

ADVANCED MATERIALS TECHNOLOGIES
www.advmattechnol.de

Ultrathin, Ultralight, and Anisotropic Ordered Reduced Graphene Oxide Fiber Electromagnetic Interference Shielding Membrane

Lu Xu, Haohao Lu, Yue Zhou, Zhangyi Chi, Zhao Li, Zahidul Islam Md, Yubing Dong, Yaqin Fu, Yaofeng Zhu, and Qingqing Ni**

Developing an electromagnetic interference (EMI) shielding material with lightweight, ultrathin, and high-performance complex electromagnetic wave pollution has become a research trend. Here, a novel ultrathin ordered reduced graphene oxide fiber (oRGOF) membranes are reported with wrinkles, grooves, and hierarchical structure by a simple assembly process based on wet spinning. The results show that the oRGOF membranes have obvious anisotropic conductivity and directional electromagnetic shielding properties. The measured electrical conductivity along the fiber axial direction (0°) is higher than that along the fiber radial direction (90°). Furthermore, the EMI shielding performance difference under different rotation angles is more than 25 dB (31.0 dB at 0°, 4.9 dB at 90°). The thickness of the resultant oRGOF membrane is 0.03 mm and area density of 0.9 mg cm^{-2}, and the specific EMI SE (SSE/t) is 33333 dB cm^2 g^{-1} along the fiber axis. The oRGOF membranes show flexible and durable performance under repeated bending and straightening cycles tests over 160 times, without significant reduction of the shielding performance. Thus, the ultrathin, ultralight, and anisotropic oRGOF electromagnetic interference shielding membrane have broad prospects for both civilian and military applications.

1. Introduction

With the gradual popularization of the fifth generation of communication technology and the extensive application of modern electronic products equipped with highly integrated circuits, electromagnetic radiation pollution has become an inevitable social problem. Thus, outstanding performance electromagnetic interference (EMI) shielding materials have drawn growing focus on the scientific community to protect the regular operation of sophisticated electronic equipment and human health.[1] Compared with traditional metal-based EMI materials as their high quality-density and poor corrosion resistance, carbonaceous EMI shielding materials such as carbon black (CB),[2] carbon nanotube (CNT),[3,4] graphene nanosheet (GNS),[5,6] and vapor-grown carbon nanofiber (VGCF)[7,8] are highly recommended by researchers due to their advantages of low density, ultrahigh mechanical properties, controllable aspect ratio, excellent electrical conductivity, and chemical stability. Especially, effective weight reduction, efficient space utilization, and energy saving are critical to applied electromagnetic protection such as in the fields of aviation and mobile devices.[9]

EMI shielding effectiveness (SE) represents the capacity of materials to suppress electromagnetic waves, usually represented in decibels (dB). Considering the applications of lightweight and ultrathin EMI SE materials, the specific EMI SE (SSE/t), SE divided by both bulk density and thickness, is a critical metric as well.[10] Many efforts had been made for the development of EMI shielding materials with light, thin, and high specific EMI SE. Zhang et al. prepared the cellulose nanofiber (CNF)/CNT composite membranes by vacuum filtration and hot pressing process, which showed 0.11 mm thickness that obtained the specific EMI SE values of 4017 dB cm^2 g^{-1} in 8–12 GHz.[11] Zhou et al. prepared CNF/ Mxene alternating multilayers with a thickness of only 0.035 mm and a specific EMI SE up to 7029 dB cm^2 g^{-1} by the repeated vacuum filtration process.[3] To obtain EMI shielding materials with better specific EMI SE, various processing techniques of carbon-based materials were developed to further improve SSE/t value under the condition of reducing thickness. Xi et al. prepared graphene aerogel films with low density (0.02 g cm^{-3}), excellent flexibility, and expansion enhancement effect by chemical reduction and high-temperature expansion. The maximum SSE/t of the material reached 22000 dB cm^2 g^{-1} in 2–18 GHz at 0.12 mm thickness.[12] Lee prepared liquid crystal GO (LCGO)/CNT composite films by spinning and multilayer assembly processes, and the SSE/t value reached 21953 dB cm^2 g^{-1} of the 0.06 mm composite films.[10] Nonetheless, the development of lightweight EMI shielding materials with ultrathin and ultrahigh SSE/t remains a daunting challenge.

L. Xu, H. Lu, Y. Zhou, Z. Chi, Z. Li, Z. I. Md, Y. Dong, Y. Fu, Y. Zhu, Q. Ni
School of Materials Science and Engineering
Zhejiang Sci-Tech University
Hangzhou, Zhejiang 310018, China
E-mail: dyb19831120@zstu.edu.cn; niqq@shinshu-u.ac.jp

The ORCID identification number(s) for the author(s) of this article can be found under https://doi.org/10.1002/admt.202100531.

DOI: 10.1002/admt.202100531

 © 2021 Wiley-VCH GmbH

In recent years, a large amount of literature have shown that the EMI shielding ability of materials is closely related to microstructure and macroscopic morphology, such as oriented structure and ordered distribution. Zeng et al. designed anisotropic CNT/water-borne polyurethane composite films with CNT-oriented structure through the facile ice-templated freeze-drying process.[13,14] Since the ordered structure of the CNT significantly improved the electrical conductivity of the materials, the EMI SE exceeded 50 dB in 8.2–12.4 GHz while the density is merely 0.126 g cm^{-3}. Moreover, Yan et al. prepared oriented VGCF/polyurethane composite films by rotating wet spinning.[15] Due to the highly oriented arrangement of VGCF, the composite films can change the EMI SE by changing the angle between the composite films and the direction of electromagnetic wave vibration.

Graphene fiber is a kind of 1D macroscopic assembly material composed of closely arranged graphene sheets. Through reasonable structural design and controllable preparation, graphene fibers can effectively transfer the excellent properties of graphene at the microscale to the macroscale, showing excellent electrical properties, and thus have great potential to be applied in EMI shielding fields.[16] In this work, we developed a simple and efficient assembly method based on wet-spinning of graphene fibers to prepare ultrathin ordered reduced graphene oxide fibers (oRGOF) membranes for directional EMI shielding. Due to the 1D microscopic oriented structure of the graphene sheets and the 2D ordered distribution of the graphene fibers, the electrical conductivity and the EMI SE of the oRGOF membranes are significantly different in different directions. Therefore, the EMI shielding performance can be adjusted by rotating the membrane angle. Furthermore, the unique wrinkles, grooves, and hierarchical structure of the membranes have a positive effect on the EMI shielding performance.

2. Results and Discussion

This study develops a novel process to assemble oriented ultrathin graphene-based membranes (see **Figure 1**). The inspiration comes from the fact of adjacent GO fibers which are easy to fuse and form a tightly connected fiber membrane. It is important to note that this fusion of fibers requires two steps. First, the GO fibers were tightly bound by water tension on the collection roller by wet spinning. Second, tightly bonded fibers were fused into films under the action of reduction and drying.

Figure 2 shows the microstructure of the disordered reduced graphene oxide fiber (dRGOF), ordered graphene oxide fiber (oGOF), and the oRGOF membranes. In contrast to the dRGOF membranes which are randomly distributed with the fibers (see Figure 2a), the fibers of the oRGOF membranes are arranged in an orderly way along the radial direction of the fibers (see Figure 2b). Several adjacent graphene fibers bond to form a larger fiber bundle. Adjacent fiber bundles are connected by one or two tilted fibers. Interestingly, this structure not only enables the fibers in the oRGOF membranes to form a whole without separation but also arrangements a dense network of conductive pathways. Furthermore, there are grooves along the axial direction of the fibers on the surface of the fibers in the film (see Figure 2d). On the one hand, this phenomenon comes from the fact that the water inside the fiber was gradually replaced by ethanol, resulting in the surface sinking of the graphite sheets.[17] On the other hand, the remaining moisture in the fibers was completely removed during the drying process, further promoting the collapse of the graphite sheets.[18] As shown in Figure 2f, axial elongation and radial contraction of the fibers under the action of axial tension led to the gradual decrease of the cross-sectional area of the fiber during the wet spinning process, and the typical microwrinkle structures of

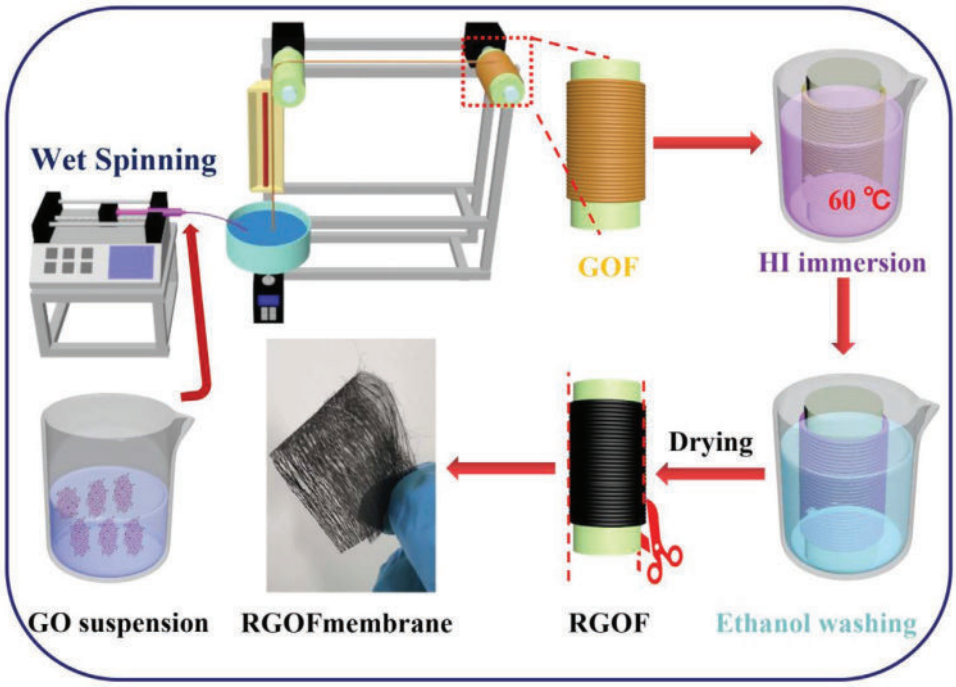

Figure 1. Schematic illustration of the fabrication process of oRGOF membranes.

© 2021 Wiley-VCH GmbH

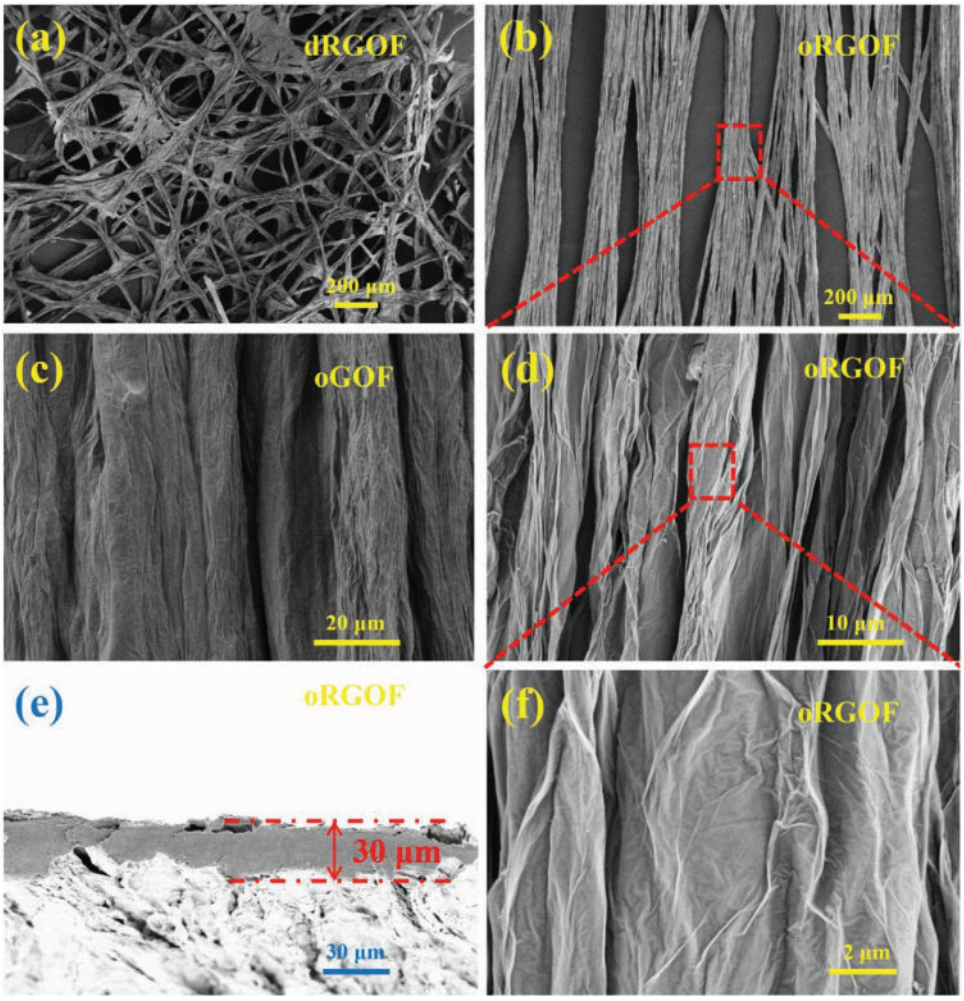

Figure 2. SEM morphology of a) dRGOF membrane, c) oGOF membrane, and b,d–f) oRGOF membrane.

graphene sheets are formed on the surface. Compared with oGOF membranes, the surface of oRGOF membranes have more grooves and wrinkles after chemical reduction. More importantly, the resulting oRGOF membranes was extremely thin, averaging 0.03 mm thick (see Figure 2c).

The formation of the oGOF membrane, dRGOF membrane, and oRGOF membrane were determined by X-ray diffraction (XRD), exhibited in **Figure 3**a. The X-ray diffraction peak of the oGOF membranes appears at $2\theta = 9.7°$, indicating that the corresponding layer spacing is approximately 0.911 nm obtained from equation $2d\sin\theta = n\lambda$.[19,20] Differently, the diffraction peak of the oRGOF membranes is at $\approx 2\theta = 24.40°$, and the corresponding graphite layer spacing is ≈0.364 nm. Since the graphite sheets are connected with oxygen-containing groups, the interlayer spacing of the oGOF membranes is distinctly greater than the oRGOF membranes. After chemical reduction, some oxygen-containing groups from the graphite sheets are removed and defects are also repaired, so agglomeration between the graphene sheets is significantly enhanced due to the strong π–π bonds. It is further confirmed that the formation of grooves and wrinkles on the surface of the membranes were closely related to chemical reduction.

To further determine more information about the graphite structures of the oGOF membrane and the oRGOF membrane during the reduction, the XPS spectrum was tested as exhibited in Figure 3b–d. Both samples contain carbon and oxygen elements according to full scan XPS spectra (see Figure 3b). The C/O atomic ratio increase from 0.95 to 2.48, indicating that C1s peak strength increased significantly and O1s peak strength decreased ominously after reduction. The C1s spectrum of the oGOF membranes can be decomposed into three characteristic peaks at 284.8 eV (C–C), 286.6 eV (C–O), and 288.2 eV (C=O), respectively.[21] Compared with the oGOF membranes, the intensity of the characteristic peaks of oxygen-containing groups in C1s pattern of the oRGOF membranes was significantly weakening (see Figure 3d). The XPS spectrum results show that the π bonding conjugate region on the GO sheets recovered and the conjugate characteristic peak strength increased after reduction. The conversion of the oGOF membranes as insulators to the oRGOF membranes as semiconductors significantly reduces the energy barrier of carrier transport and improves the electrical conductivity of the membranes.

The Raman spectral analysis of the oGOF membrane, dRGOF membrane, and oRGOF membrane are shown in

© 2021 Wiley-VCH GmbH

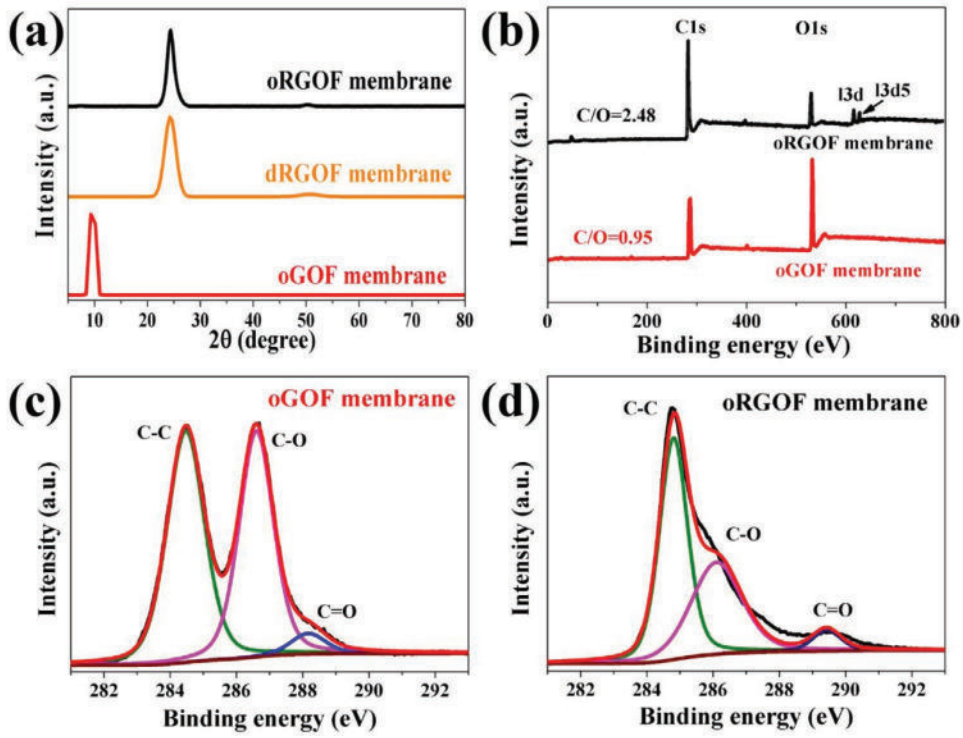

Figure 3. a) XRD patterns of oGOF, dRGOF, and oRGOF membranes; b–d) XPS Spectra of oGOF and oRGOF membranes.

Figure 4a. Similarly, the three samples both produce strong characteristic peaks at 1345 and 1585 cm^{-1}.[22] It should be noted that the associated D and G bands indicate the defect structure and graphite structure of graphene respectively.[23] The lower I_D/I_G values of the dRGOF membranes and oRGOF membranes reflect that the dRGOF membranes and oRGOF membranes have fewer structural defects and a more orderly structure than oGOF membranes.[24]

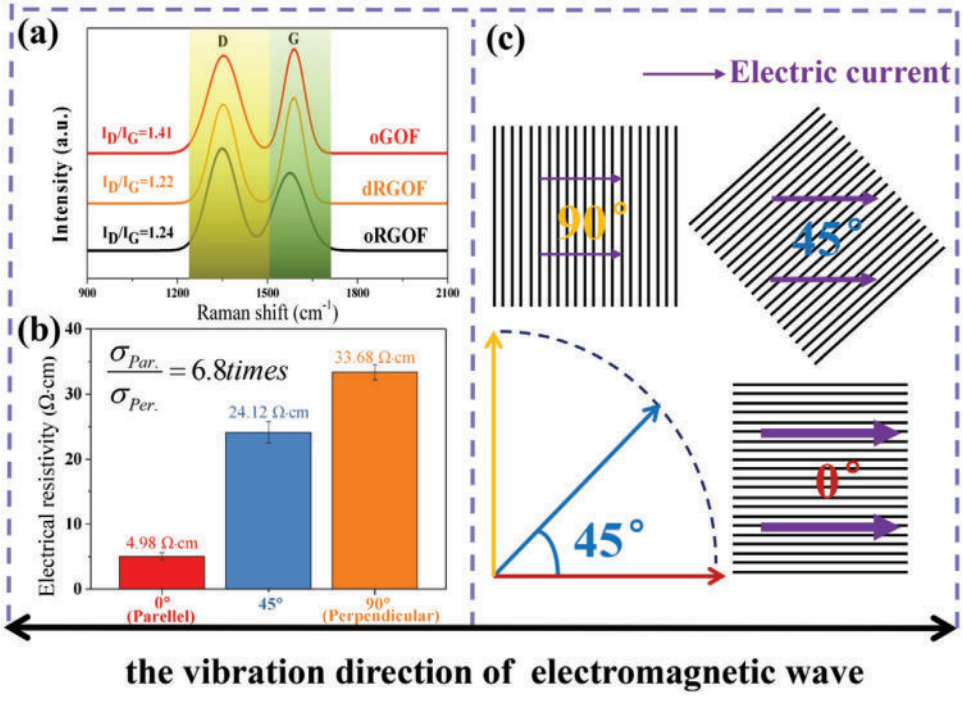

Figure 4. a) Raman spectra of oRGOF, dRGOF, and oGOF membrane; b) Electrical resistivity (σ^{-1}) of oRGOF membranes at 0°, 45°, and 90°; c) Angular difference between the fiber axes directions and the vibration direction of the electromagnetic wave.

© 2021 Wiley-VCH GmbH

The electrical resistivities (σ^{-1}) of the oRGOF membranes at 0°, 45°, and 90° are shown in Figure 4b. The testing process are detailed as shown in Figure S4 (Supporting Information). For an individual graphene fiber, the graphene sheets are arranged in parallel along the fiber axis and the distance between the layers is maintained at 0.335 nm.[25–27] The P_z orbital electrons interact with each other perpendicular to the plane of the structural layer to form the conjugated π bonds. Since the π bonds are semifilled, electrons can move freely within the structural layer. The relevant literature demonstrated that the enhanced alignment of the graphene sheets provides an efficient electron-conducting path for electron conduction along the fiber axis.[28,29] Therefore, graphene fibers have excellent electrical conductivity in the axial direction of the fibers. In contrast, the graphene sheets show a bending strain in the radial direction of the fibers. Hicks et al. found that the bending strain of graphene sheets would destroy the interaction between π orbitals, forming a bandgap with an energy greater than 0.5 eV and impeding electron transport between graphene sheets.[30] Therefore, the electrical conductivity of graphene fiber in the axial direction is better than that in the radial direction, that is, graphite fiber has anisotropic conductivity. The oRGOF membrane assembled from graphene fibers is undoubtedly inheriting the conductive properties of graphene fibers. Furthermore, the many larger elongated holes generated by the ordered distribution of graphene fibers along the radial direction of the fibers make the electron transport pathway much longer, further enlarging the difference in the conductivity of the oRGOF membranes along parallel and perpendicular to the graphene fiber axis. Macroscopically, the oRGOF membranes have anisotropic electrical conductivity, and the electrical conductivity of oRGOF membranes parallel to the fiber axis (0°) is 6.8 times that of the oRGOF membranes perpendicular to the fiber axis (90°).

To explore the effect of anisotropic electrical conductivity on EMI shielding performance, the EMI SE of the directional oRGOF membranes was evaluated by changing the angle of rotation of the membranes to change the vibration direction of electromagnetic wave (see Figure 4c). The total shielding performance (SE_T), reflection loss (SE_R), and absorption loss (SE_A) of the oRGOF membranes with different directions in 8.2–12.4 GHz are shown in **Figure 5**. The maximum SE_T value of the oRGOF-0° is up to 31.0 dB, that is, a shielding efficiency of 99.9%. By comparison, the maximum SE_T value is the oRGOF-90° only 4.9 dB. The EMI shielding performance difference of the oRGOF membranes along the parallel and perpendicular fiber axes is up to 25 dB. This result is consistent with the big difference in the electrical conductivity of the films along the parallel and perpendicular fiber axes. The maximum SE_T value of the oRGOF-45° and dRGOF are 14.9 and 20.5 dB, respectively, both of which were less than the SE_T value of oRGOF-0°. Similarly, the electrical conductivity of both is less than that of oRGOF-0°. This proves that the anisotropic electrical conductivity plays a key role in the directional EMI shielding performance. A further illustration of the role of conductivity in shielding is shown in **Figure 6**a. According to the circuit theory, surface current density was formed on the surface of the oRGOF membranes when the electromagnetic wave encounters the oRGOF membranes. Then the surface current

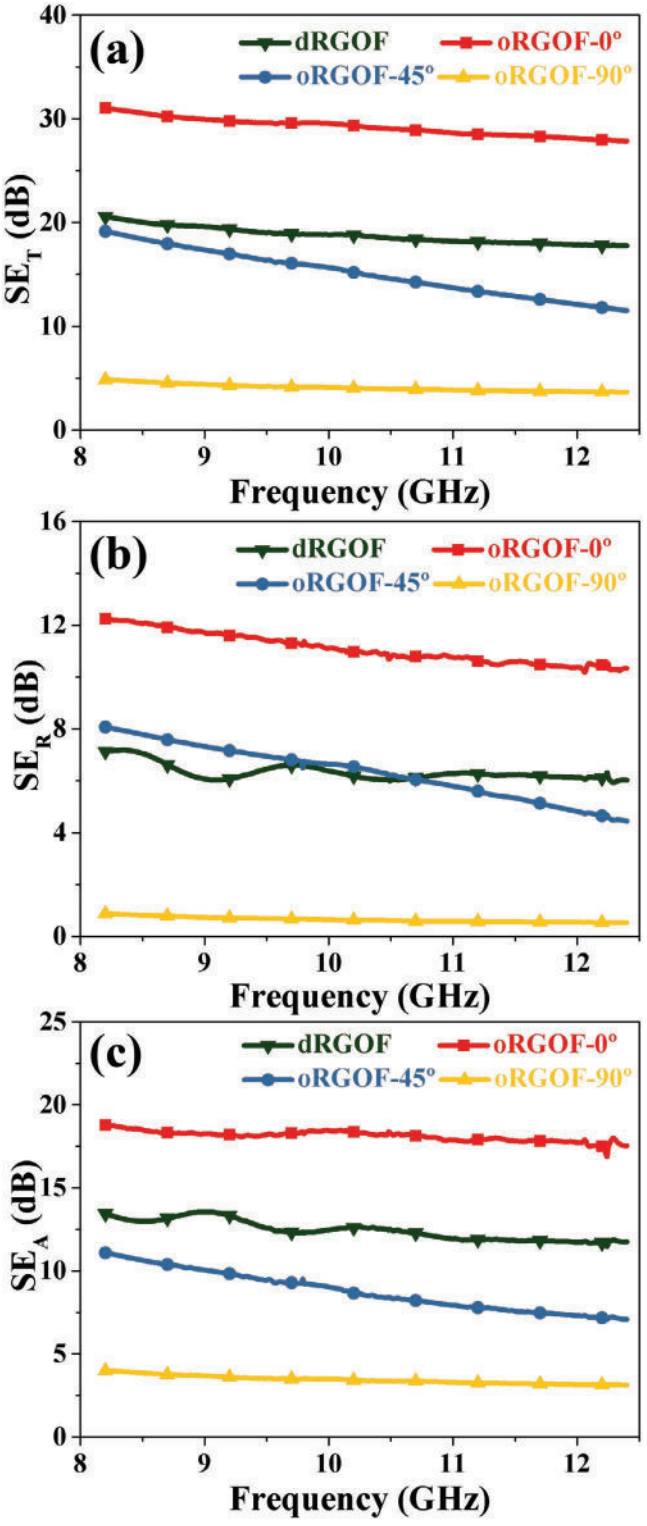

Figure 5. Plots of a) SE_T, b) SE_R, and c) SE_A of the membranes.

density onto the oRGOF membranes will generate a magnetic field (H) perpendicular to it, and the magnetic field would create an opposite electromotive force, which can attenuate the current to penetrate the oRGOF membranes. This phenomenon

© 2021 Wiley-VCH GmbH

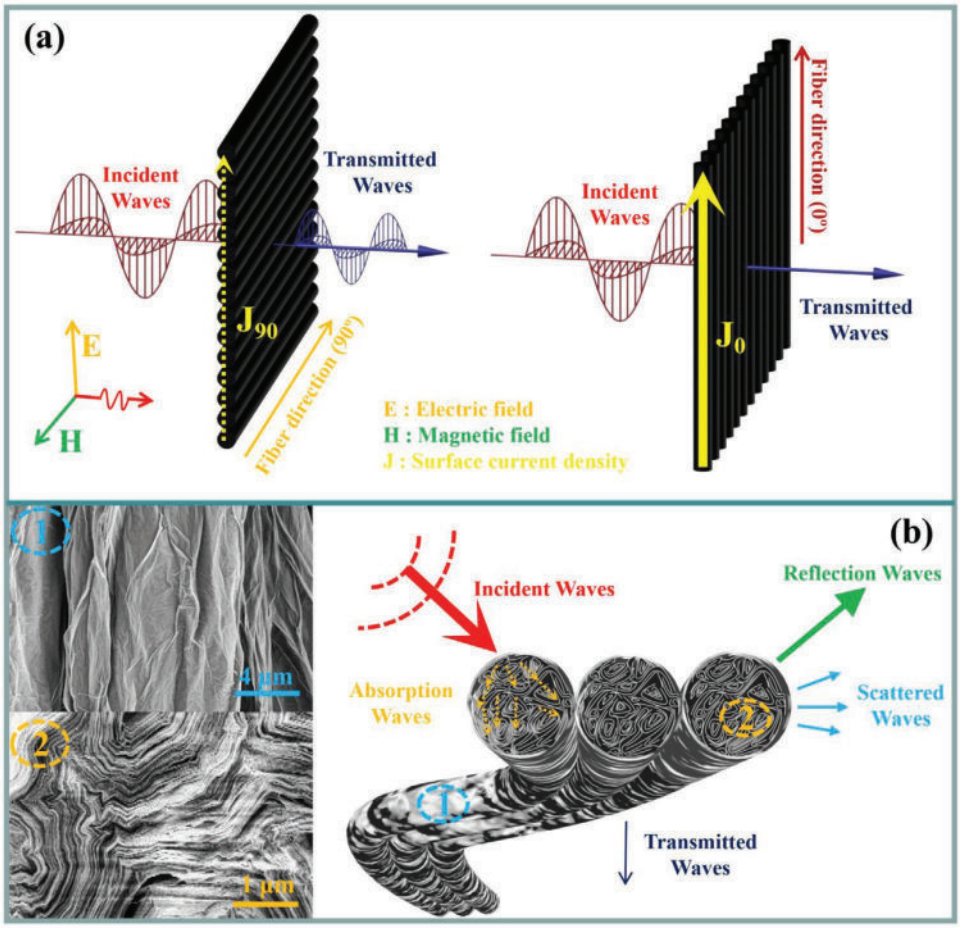

Figure 6. a) Schematic diagram of directional EMI shielding; b) Schematic diagram of microstructure of oRGOF membranes.

leads to the attenuation of electromagnetic waves. The surface of the oRGOF-0° can generate a larger current surface density to effectively attenuate the incident electromagnetic wave when the direction of the electric field in the electromagnetic wave is parallel to the fiber axis. Moreover, some literature have shown that the ordered distribution of carbon-based fibers (including carbon fiber[15] and CNT yarn[31]) along the radial direction of the fibers can produce materials with directional EMI shielding properties.

The microscopic structures of the oRGOF membranes, such as wrinkles, grooves and, hierarchical structures, are also one of the factors affecting EMI shielding performance.[32,33] A schematic diagram of the relationship between the EMI shielding mechanism and the microstructure of the oRGOF membranes is shown in Figure 6b. By investigating the SE_T value of 31.0 dB obtained from the oRGOF membranes, ≈18.8 dB of electromagnetic attenuation was due to absorption loss, 12.2 dB to reflection loss, as shown in Figure 5a-c. In other words, more than the 90% of electromagnetic wave is reflected and almost 99% percent of left less than 10% electromagnetic wave is absorbed by oRGOF membranes. Particularly, the availability of the oRGOF membranes in absorbing the incoming electromagnetic wave was closely related to the hierarchical structures of graphene sheets. These structures effectively lengthen the path of incoming electromagnetic waves through the membranes, allowing the incoming electromagnetic waves to be attenuated by absorption and multiple reflections, among graphite sheets in the oRGOF membranes.[34–37] Moreover, the grooves and wrinkles on the surface of the oRGOF membranes are beneficial to the interfacial scattering of the electromagnetic waves, and improving EMI shielding performance.[38]

The SE_T values of all the membrane samples decreased with the increase of frequency. This is because the resistance and reactance of the membranes increase with increasing frequency, resulting in the weakening of the electromagnetic wave reflection ability of the membranes. This is consistent with the experimental results that the SE_R value decreases with increasing frequency. Furthermore, there is the presence of so many larger elongated holes in the fiber direction. Each elongated hole can be regarded as a small rectangular waveguide tube, and the membrane has a cut-off frequency (which is related to the geometry of the elongated hole). As the test frequency approaches the cut-off frequency, the number of electromagnetic waves passing through the membrane increases, which reduces the shielding performance.

As an integrated graphene assembly material, the electronic transport performance of the ultrathin oRGOF membranes is affected by bending deformation.[39] The resistance

© 2021 Wiley-VCH GmbH

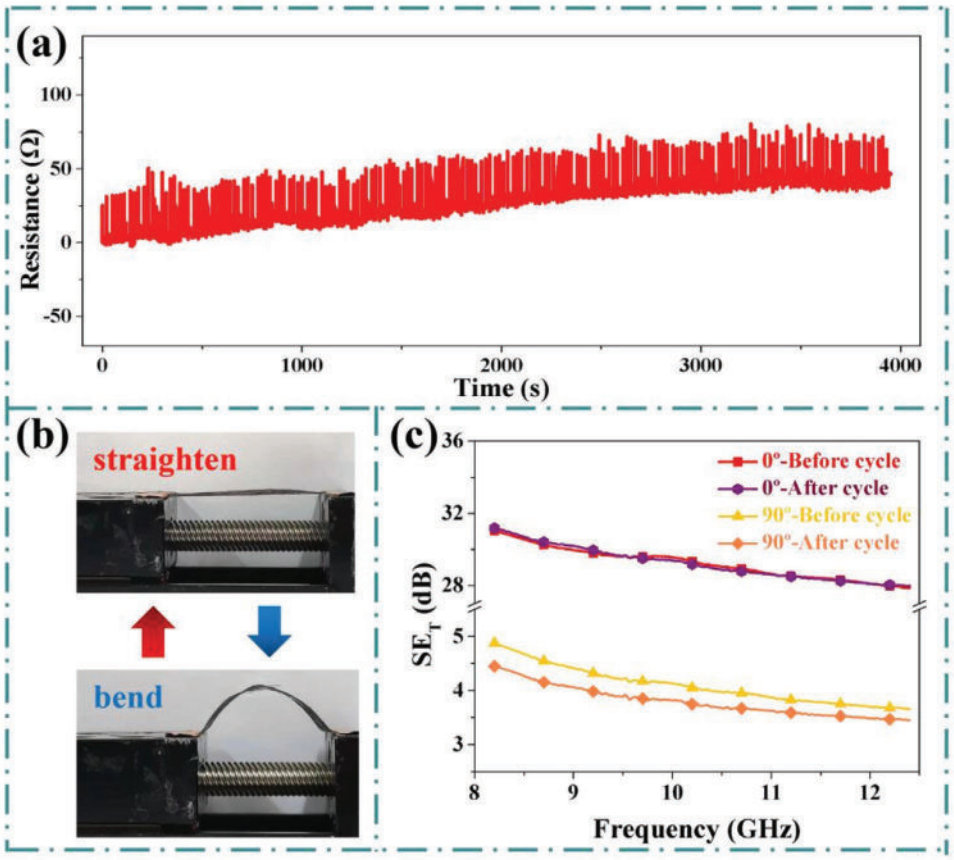

Figure 7. a) Resistance change curve of oRGOF membranes under the bending–straightening cycles; b) Bending and straightening cycles movement of oRGOF membranes driven by the motor controlled screw sliding table device; c) EMI shielding properties of oRGOF membranes before and after bending and straightening 160 cycles.

change curve of the oRGOF membranes was tested under the bending–straightening cycles, as shown in **Figure 7**a. The range of the oRGOF membrane's resistance changed from 0.9–25.0 Ω at the beginning to 37.7–71.8 Ω at a screw sliding speed of 30 mm min^{-1} after 160 bending–straightening cycles. Very few hierarchical structures of graphene sheets were demolished in the process of continuous bending, resulting in a gradual increase of the resistance of the oRGOF membranes. Nevertheless, the SE_T value along the fiber axial direction at 8.2–12.4 GHz hardly changed before and after 160 bending–straightening cycles, indicating the stable EMI shielding performance of the oRGOF membranes (see Figure 7c). Besides, the oRGOF membranes have good flexibility, and their macroscopic shape remained as before during the process of straightening and bending.

To emphasize the efficient EMI SE of the oRGOF membranes, the SSE/t of EMI shielding materials in the latest document is listed in **Figure 8**.[40–45] The oRGOF membranes mentioned have a higher SSE/t (33333 dB cm^2 g^{-1}) along the fiber axial direction, which is much higher than other materials presented in Figure 8. This prominent feature is mainly due to unique orientation, hierarchical structures of graphite sheets and ordered distribution of graphite fibers, demonstrating the superiority of ultrathin microstructure in EMI shielding materials.

3. Conclusions

In this present work, anisotropic and ultrathin oRGOF membranes with excellent EMI shielding performance were prepared by a novel assembly method based on wet-spinning. The results show that the structures of the membranes are the main

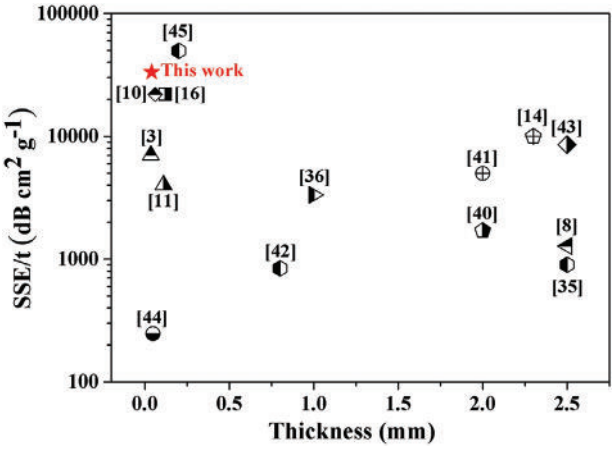

Figure 8. Comparison of SSE/t and thickness of oRGOF membranes with the other materials.

© 2021 Wiley-VCH GmbH

factors affecting the conductivity and EMI shielding properties. On the one hand, the axial orientation of graphene sheets and the ordered distribution of graphene fibers make the oRGOF membranes anisotropy conductivity and directional EMI shielding. The EMI SE difference along the fiber radial direction and the fiber axial direction of the oRGOF membranes with a thickness of 0.03 mm and area density of 0.9 mg cm^{-2} is more than 25 dB. On the other hand, the wrinkles, grooves, and hierarchical structure of the oRGOF membranes formed by chemical reduction and drying processes effectively have a positive effect on the EMI SE. The specific EMI SE (SSE/t) of the oRGOF membranes was 33333 dB cm^2 g^{-1} along the fiber axis. Furthermore, the oRGOF membranes show flexible and durable performance under repeated bending and straightening cycles tests over 160 times, without significant reduction of the shielding effectiveness. Therefore, the ultrathin oRGOF membranes with characteristic microstructure have great potential to be used in the field of mobile devices and wearable devices for eliminating electromagnetic noise, interfering electromagnetic waves, and precise filtering electromagnetic waves.

4. Experimental Section

Materials: Large-size graphene oxide slurry (GO, solid concentration = 1%, sheet diameter = 5–40 μm) was obtained from Ang Xing Novel Carbon Material Co. LTD, China. Calcium chloride ($CaCl_2$) and absolute ethanol (C_2H_6O, liquid concentration ≥ 99.7%), and hydroiodic acid aqueous solution (HI, liquid concentration = 40%) was purchased from Aladdin Reagent, China. Ultrapure water was obtained from commercial sources.

Preparation of oRGOF Membranes: The oRGOF membranes were fabricated by a two-step wet spinning/chemical reduction, as shown in Figure 1. First, 3 wt% high concentration GO spinning suspension was purified by 1 wt% GO aqueous suspension at a centrifugal speed of 18 000 r min^{-1} and a centrifugal time of 2 h. Then, the resulting spinning liquid was packed into a 10 mL glass needle tube with an aperture of 90 μm. Second, the oGOF are collected into rollers during the wet-spinning process. The coagulated bath solution was composed of $CaCl_2$, ethanol, and water (5 wt% $CaCl_2$, a volume ratio of ethanol to water = 1:3). Third, the oGOF was reduced to oRGOF by immersion in HI solution at 60 °C for 4 h. Then the oRGOF was rinsed with ethanol until the I_2 is completely removed from the surface. Finally, the oRGOF were placed in a vacuum drying chamber at 60 °C and then cut to obtain a complete oRGOF membrane. The surface density of the oRGOF membrane was 0.9 mg cm^{-2}.

Preparation of dRGOF Membranes: Similar to the above steps, 3 wt% GO aqueous suspension was prepared into GO fibers (GOF) by the wet spinning process. In contrast, the irregularly distributed GOF were collected directly in a rotating solidification bath rather than on a roller. After that, the Brucellae funnel was used to extract the coagulation bath solution, and the disordered GOF (dGOF) membranes were obtained. Finally, dGOF membranes were reduced to dRGOF membranes through the same reduction process. It should be pointed out that the surface density of the dRGOF membranes was similar to that of oRGOF membranes.

Characterization: The microstructures of the membranes were observed by scanning electron microscope (SEM, Ultra 55, Zeiss). The chemical structures of the oGOF membranes and oRGOF membranes were analyzed by Raman spectrometer (Renishaw 2000), X-ray photoelectron spectroscopy (XPS, Thermo Scientific K-Alpha), and XRD (Bruker advance D8). The electrical resistivity of the membranes was measured through the four-probe method using a probe station (SZT-2B). The EMI SE of the samples was tested according to the standard waveguide method using a vector network analyzer (N522A, Keysight) (see Figure S1 in the Supporting Information). The bending and straightening cycle tests of the oRGOF membranes were performed using the self-assembly motor-controlled screw sliding table device, and the resistance of the oRGOF membranes was tested using a multifunctional electrometer (Keithley 6514) with matching measurement software.

Supporting Information

Supporting Information is available from the Wiley Online Library or from the author.

Acknowledgements

This work was supported by the National Natural Science Foundation of China (Grant No. 52073259), Joint Funds of the National Natural Science Foundation of China (Grant No. U20A20264), Project funded by China Postdoctoral Science Foundation (Grant No. 2021M692864), Zhejiang Provincial Natural Science Foundation of China (Grant No. LY19E030010), and Professional Degree Postgraduate Training Mode Reform Project (Grant No. Y202045462).

Conflict of Interest

The authors declare no conflict of interest.

Data Availability Statement

Research data are not shared.

Keywords

graphene, electromagnetic interference shielding, electrical properties, anisotropy

Received: May 5, 2021
Revised: July 22, 2021
Published online:

[1] B. Y. Wen, X. J. Wang, Y. Zhang, *Compos. Sci. Technol.* **2019**, *169*, 127.
[2] M. H. Al-Saleh, W. H. Saadeh, U. Sundararaj, *Carbon* **2013**, *60*, 146.
[3] B. Zhou, Z. Zhang, Y. L. Li, G. J. Han, Y. Z. Feng, B. Wang, D. B. Zhang, J. M. Ma, C. T. Liu, *ACS Appl. Mater. Interfaces* **2020**, *12*, 4895.
[4] Q. Song, F. Ye, X. W. Yin, W. Li, H. J. Li, Y. S. Liu, K. Z. Li, K. Y. Xie, X. H. Li, Q. G. Fu, L. F. Cheng, L. T. Zhang, B. Q. Wei, *Adv. Mater.* **2017**, *29*, 1701583.
[5] J. Q. Ling, W. T. Zhai, W. W. Feng, B. Shen, J. F. Zhang, W. G. Zheng, *ACS Appl. Mater. Interfaces* **2013**, *5*, 2677.
[6] B. Shen, W. T. Zhai, W. G. Zheng, *Adv. Funct. Mater.* **2015**, *24*, 4542.
[7] D. D. L. Chung, *Carbon* **2012**, *50*, 3342.
[8] X. H. Hong, D. D. L. Chung, *Carbon* **2017**, *111*, 529.
[9] S. H. Lee, D. Kang, I. K. Oh, *Carbon* **2017**, *111*, 248.
[10] D. W. Lee, H. Kim, J. S. Hyeon, J. H. Moon, B. J. Kim, J. H. Jeong, J. Choi, R. H. Baughman, G. M. Spinks, G. G. Wallace, S. J. Kim, *ACS Appl. Mater. Interfaces* **2020**, *12*, 46883.
[11] H. R. Zhang, X. W. Sun, Z. G. Heng, Y. Chen, H. W. Zou, M. Liang, *Ind. Eng. Chem. Res.* **2018**, *57*, 17152.

 © 2021 Wiley-VCH GmbH

[12] J. B. Xi, Y. L. Li, E. Z. Zhou, Y. J. Liu, W. W. Gao, Y. Guo, J. Ying, Z. C. Chen, G. G. Chen, C. Gao, *Carbon* **2018**, *135*, 44.
[13] Z. H. Zeng, H. Jin, M. J. Chen, W. W. Li, L. C. Zhou, Z. Zhang, *Adv. Funct. Mater.* **2016**, *26*, 303.
[14] Z. H. Zeng, H. Jin, M. J. Chen, W. W. Li, L. C. Zhou, X. Xu, Z. Zhang, *Small* **2017**, *13*, 1701388.
[15] Y. J. Yan, H. Xia, Y. P. Qiu, Z. Z. Xu, Q. Q. Ni, *Mater. Lett.* **2019**, *245*, 98.
[16] S. H. Chen, W. J. Ma, Y. H. Cheng, Z. Weng, B. Sun, L. Wang, *Nano Energy* **2015**, *15*, 642.
[17] H. H. Cheng, J. Liu, Y. Zhao, C. G. Hu, Z. P. Zhang, N. Chen, *Angew. Chem., Int. Ed.* **2013**, *52*, 10482.
[18] R. Jalili, S. H. Aboutalebi, D. Esrafilzadeh, R. L. Shepherd, J. Chen, S. Aminorroaya-Yamini, K. Konstantinov, A. I. Minett, J. M. Razal, G. G. Wallace, *Adv. Funct. Mater.* **2013**, *23*, 5345.
[19] L. Chen, L. Y. He, S. G. Chai, H. Qiang, F. Chen, Q. Fu, *Nanoscale* **2013**, *5*, 5809.
[20] Z. Xu, C. Gao, *Nat. Commun.* **2011**, *2*, 571.
[21] Y. L. Xu, A. Uddin, D. Estevez, Y. Luo, H. X. Pen, F. X. Qin, *Compos. Sci. Technol.* **2020**, *189*, 108022.
[22] Y. S. Choi, C. S. Yeo, S. J. Kim, J. Y. Lee, Y. Kim, K. R. Cho, *Nanoscale* **2019**, *11*, 12637.
[23] F. Y. Liu, Y. B. Dong, R. K. Shi, E. L. Wang, Q. Q. Ni, Y. Q. Fu, *Mater. Today Commun.* **2020**, *24*, 100909.
[24] Y. Li, X. L. Pei, B. Shen, W. T. Zhai, L. H. Zhang, W. G. Zheng, *RSC Adv.* **2015**, *5*, 24342.
[25] J. K. Mu, C. Y. Hou, G. Wang, X. M. Wang, Q. H. Zhang, Y. G. Li, *Adv. Mater.* **2016**, *28*, 9491.
[26] Z. Xu, H. Y. Sun, X. L. Zhao, C. Gao, *Adv. Mater.* **2013**, *25*, 188.
[27] L. Z. Sheng, T. Wei, Y. Liang, L. L. Jiang, L. T. Qu, Z. J. Fan, *Carbon* **2017**, *120*, 17.
[28] L. Chen, Y. L. He, S. G. Chai, H. Qiang, F. Chen, Q. Fu, *Nanoscale* **2013**, *5*, 5809.
[29] G. Q. Xin, W. G Zhu, Y. X. Deng, J. Cheng, L. T. Zhang, A. J. Chung , S. De, J. Lian, *Nat. Nanotechnol.* **2019**, *14*, 168.
[30] J. Hicks, A. Tejeda, A. Taleb-Ibrahimi, M. S. Nevius, F. Wang, K. Shepperd, J. Palmer, F. Bertran, P. Le Fèvre, J. Kunc1, W. A. de Heer, C. Berger, E. H. Conrad, *Nat. Phys.* **2013**, *9*, 49.
[31] N. Chikyu, T. Nakano, G. Kletetschka, Y. Inoue, *Mater. Des.* **2020**, *195*, 108918.
[32] Z. Yu, T. W. Dai, S. W. Yuan, H. W. Zou, P. B. Liu, *ACS Appl. Mater. Interfaces* **2020**, *12*, 30990.
[33] Z. Xu, Y. J. Liu, X. L. Zhao, L. Peng, H. Y. Sun, Y. Xu, *Adv. Mater.* **2016**, *28*, 6449.
[34] M. S. Cao, X. X. Wang, W. Q. Cao, J. Yuan, *J. Mater. Chem. C* **2015**, *3*, 6589.
[35] N. Yousefi, X. Y. Sun, X. Y. Lin, X. Shen, J. J. Jia, B. Zhang, B. Z. Tang, M. S. Chan, J. K. Kim, *Adv. Mater.* **2014**, *26*, 5480.
[36] D. X. Yan, H. Pang, B. Li, R. Vajtai, L. Xu, P. G. Ren, J. H. Wang, Z. M. Li, *Adv. Funct. Mater.* **2015**, *25*, 559.
[37] Z. P. Chen, X. Cu, C. Q. Ma, W. C. Ren, H. M. Cheng, *Adv. Mater.* **2015**, *25*, 1296.
[38] X. H. Li, X. F. Li, K. N. Liao, P. Min, T. Liu, A. Dasari, Z. Z. Yu, *ACS Appl. Mater. Interfaces* **2016**, *8*, 33230.
[39] L. Y. Liang, P. H. Xu, Y. F. Wang, Y. Shang, J. M. Ma, F. M. Su, Y. Z. Feng, C. G. He, Y. M. Wang, C. T. Liu, *Chem. Eng. J.* **2020**, *395*, 125209.
[40] M. Liu, S. Roy, E. K. Chu, K. Y. See, X. Hu, *ACS Appl. Mater. Interfaces* **2016**, *8*, 7422.
[41] Y. Chen, H. B. Zhang, Y. B. Yang, M. Wang, A. Y. Cao, Z. Z. Yu, *Adv. Funct. Mater.* **2016**, *26*, 447.
[42] N. Agnihotri, K. Chakrabarti, A. De, *RSC Adv.* **2015**, *5*, 43765.
[43] M. Z. Li, L. C. Jia, X. P. Zhang, D. X. Yan, Q .C. Zhang, Z. M. Li, *J. Colloid Interface Sci.* **2018**, *530*, 113.
[44] W. T. Cao, F. F. Chen, Y. J. Zhu, Y. G. Zhang, Y. Y. Jiang, M. G. Ma, F. Chen, *ACS Nano* **2018**, *12*, 4583.
[45] D. G. Lai, X. X. Chen, Y. Wang, *Carbon* **2020**, *158*, 728.

© 2021 Wiley-VCH GmbH